

1 **Title: Universality of clone dynamics during tissue development**

2 **Authors:** Steffen Rulands^{1-5,*}, Fabienne Lescroart⁶, Samira Chabab⁶, Christopher J. Hindley^{1,2},
3 Nicole Prior², Magdalena K. Sznurkowska^{2,7}, Meritxell Huch^{2,3}, Anna Philpott^{2,7}, Cedric
4 Blanpain⁶ and Benjamin D. Simons^{1-3,*}

5 **Affiliations:**

6 ¹Cavendish Laboratory, Department of Physics, JJ Thomson Avenue, University of Cambridge,
7 Cambridge CB3 0HE, UK.

8 ²The Wellcome Trust/Cancer Research UK Gurdon Institute, University of Cambridge, Tennis
9 Court Road, Cambridge CB2 1QN, UK.

10 ³Wellcome Trust Centre for Stem Cell Research, University of Cambridge, Tennis Court Road,
11 Cambridge CB2 1QR, UK.

12 ⁴Max Planck Institute for the Physics of Complex Systems, Noethnitzer Str. 38, 01187 Dresden
13 Germany

14 ⁵Center for Systems Biology Dresden, Pfotenhauer Str. 108, 01307 Dresden, Germany

15 ⁶Université Libre de Bruxelles, Laboratory of Stem Cells and Cancer, Brussels B-1070, Belgium.

16 ⁷Department of Oncology, University of Cambridge, Hutchison/MRC Research Centre, Hills
17 Road, Cambridge CB2 0XZ, UK.

18 * Corresponding authors

19 **The emergence of complex organs is driven by the coordinated proliferation, migration and**
20 **differentiation of precursor cells. The fate behaviour of these cells is reflected in the time**
21 **evolution their progeny, termed clones, which serve as a key experimental observable. In**
22 **adult tissues, where cell dynamics is constrained by the condition of homeostasis, clonal**
23 **tracing studies based on transgenic animal models have advanced our understanding of cell**
24 **fate behaviour and its dysregulation in disease (1, 2). But what can be learned from clonal**
25 **dynamics in development, where the spatial cohesiveness of clones is impaired by tissue**
26 **deformations during tissue growth? Drawing on the results of clonal tracing studies, we**
27 **show that, despite the complexity of organ development, clonal dynamics may converge to**
28 **a critical state characterized by universal scaling behaviour of clone sizes. By mapping**
29 **clonal dynamics onto a generalization of the classical theory of aerosols, we elucidate the**
30 **origin and range of scaling behaviours and show how the identification of universal scaling**
31 **dependences may allow lineage-specific information to be distilled from experiments. Our**
32 **study shows the emergence of core concepts of statistical physics in an unexpected context,**
33 **identifying cellular systems as a laboratory to study non-equilibrium statistical physics.**

34

35 Biological systems, being highly structured and dynamic, function far from thermal equilibrium.
36 This is particularly evident in embryonic development where, through large-scale cellular self-
37 organisation, highly complex structures emerge from a group of genetically identical, pluripotent
38 stem cells. To achieve the stereotypic ordering of organs and tissues, the fate of embryonic stem
39 cells and their progeny must be tightly-regulated, such that the correct number and type of cells
40 is generated at the right time and place during development. Mechanisms regulating such cell
41 fate decisions are at the center of research in stem cell and developmental biology (3). Efforts to

42 resolve the mechanisms that regulate cell fate behaviour place emphasis on emerging
43 technologies, including single-cell genomics and genome editing methods, which provide
44 detailed information on the subcellular and cellular processes. However, by focusing on gene
45 regulatory programmes, such approaches often fail to engage with how collective cell behaviour,
46 and the formation of functioning organs, emerges from the network of complex interactions at
47 the molecular scale.

48 To understand how complexity at the microscopic scale translates into coherent collective
49 behaviour at the macro-scale, statistical physics provides a useful theoretical framework. For
50 critical systems, where fluctuations are scale-invariant, successive coarse-graining can yield
51 effective theories describing macroscopic behavior. In such systems, different “microscopic”
52 systems can give rise to indistinguishable macroscopic behavior – a concept known as
53 universality. As a reflection of scale invariance, statistical correlations, such as size distributions,
54 obtain simple scaling forms, which depend only on one or few dimensionless composite
55 variables. But, given the complexity of embryonic development, can such concepts be applied to
56 study cellular behaviour?

57 At the cellular scale, the patterns of cell fate decisions during embryonic development are
58 reflected in the time-evolution of individual developmental precursors cells and their progeny,
59 which together constitute a clone. While the dynamics of individual clones maybe complex,
60 subject both to intrinsic and extrinsic influences, statistical ensembles of clones may provide
61 robust (predictive) information about the relationship between different cell types and
62 mechanisms regulating cellular behaviour. In mammals, where live-imaging of developing
63 embryonic organs is typically infeasible, efforts to resolve clonal dynamics have relied on cell
64 lineage tracing studies using transgenic animal models (*1*). In this approach, the activation of a

65 reporter gene allows individual cells to be marked with a fluorescent reporter. As a genetic mark,
66 this label is then inherited by all progeny of a marked cell, and allows clone sizes and cell
67 compositions to be recorded at specific times post-labelling (Figure 1A). Lineage tracing studies
68 therefore provide a “two-time” measure of clonal dynamics in the living embryo. In adult tissues,
69 where cell dynamics is heavily constrained by the steady state condition of homeostasis, efforts
70 to resolve cell fate behaviour from clonal tracing studies have drawn successfully upon concepts
71 from statistical physics and mathematics (4–6). However, in developing tissues, the
72 interpretation of these experiments is complicated by the fact that clonal dynamics is, in
73 principle, less constrained. Moreover, due to large-scale cellular rearrangements as well as
74 stochastic forces from surrounding tissues, labelled clones may fragment into disconnected
75 clusters, or they merge and form larger compounds of labelled cells (Figure 1B-F).

76 Here, by establishing a formal mapping between clonal dynamics and a generalization of
77 the theory of aerosols, we show that, during embryonic development, clonal dynamics converges
78 to a critical state, giving rise to universal scaling behaviour of the size distributions of labelled
79 clusters. Further, we explore how understanding the origins of scaling and universality can form
80 the quantitative basis for recovering information on cell fate behaviour during development. We
81 thus find the emergence of core concepts of statistical physics in the unexpected context of
82 embryonic development. As well as being of interest in the study of tissue development, these
83 findings have important implications for the study of tissue regeneration and tumour growth.

84 To develop this programme, we begin with an example of clonal evolution during the
85 development of mouse heart. The gene *Mesp1* is transiently expressed between embryonic day
86 (E)6.5 and E7.5 in mice in the earliest precursor cells of the heart (7–9). Quantitative analysis of
87 hearts labelled at low density (1-2 clones per heart) have established the temporal progression in

88 differentiation and proliferative capacity of these precursors (8, 9). However, with just 1 or 2
89 clones per embryo, and inherent variability in the efficiency of labelling, low-density labelling is
90 highly inefficient in probing evolutionary processes during development. By contrast, at high
91 (mosaic) labelling density, each embryo provides a potentially rich dataset. The situation is
92 exemplified in Figure 1E, which shows mouse hearts at E12.5 and postnatal day P1 after mosaic
93 labelling between E6.5 and E7.5 using the multicolour *Mesp1-Cre/Rosa-Confetti* reporter
94 construct (with 50% of the cardiac surface being fluorescently labelled with each of three
95 colours, cyan, yellow and red, roughly equally represented). However, at this density of
96 labelling, a single contiguous cluster of labelled cells can be derived from the chance fusion of
97 two or more independent clones induced with the same colour (10). Given that clone sizes are
98 not constrained by tissue size, and the ambiguity arising from clone merger and fragmentation, to
99 what extent can information on cell fate behaviour be recovered?

100 To address this question, we quantified the surface area (SA) covered by each cluster in a
101 given heart compartment at different developmental time points. From the SAs, we then
102 determined their distributions in each heart region (Fig. 1F). Although cardiac development
103 involves complex cell fate decisions, with regional and temporal variations in proliferation (11,
104 12), we found that the resulting cluster size distribution was remarkably conserved: After
105 rescaling the SA of each cluster by the ensemble average for each compartment at a given time
106 point, the resulting rescaled size distributions perfectly overlapped (Fig. 1G,H). This result
107 implies that, despite the complex and variable histories, the resulting SA distribution is fully
108 characterized by the average alone, the defining property of scaling. Formally, the frequency
109 $f(x, t)dx$ of a cluster with a SA between x and $x + dx$ at time t post-labelling acquires the
110 statistical scaling form, $f(x, t) = \phi(x/\langle x(t) \rangle)$, where ϕ denotes the scaling function.

111 The simplicity of the cluster size distribution that is reflected in scaling behaviour
112 suggests that its origin may not rely on details of the morphogenic programme in heart. Rather,
113 to uncover its origin, we began by considering the simplest set of processes that could determine
114 cluster size: First, as labelled cells divide, clusters may grow at a rate proportional to their size.
115 Second, in expanding tissues, clones may fragment into disconnected clusters as cells disperse or
116 the tissue deforms. If the rate of growth and fragmentation increase in proportion to cluster size,
117 the SA distribution would be predicted to become stationary. However, although clonal tracing
118 studies indicate that growth and fragmentation occur on a similar time scale during the early
119 phase of heart development (E6.5 and E12.5) (9), average cluster sizes at E12.5 and P1 differ by
120 a factor of 2.7, showing that steady-state is not reached. More importantly, such a simple line of
121 argument neglects the possibility that clusters of the same colour can merge into larger,
122 cohesively labelled regions. Yet the number of clusters varies only marginally between E12.5
123 and P1 (9), indicating that merger and fragmentation could be equally abundant.

124 To resolve the origin of scaling, it is instructive to leave temporarily the realm of biology
125 and consider the growth dynamics of “inanimate” compounds. Indeed, processes involving
126 merger and fragmentation occur in multiple contexts in physics, including the nucleation of
127 nano-crystals, amyloid fibrils, polymerisation, endocytosis and the dynamics of aerosols (13–16).
128 In common with clonal evolution in tissues, droplets in aerosols may merge (coagulate) or they
129 may fragment (Fig. 2A). By analogy with clonal growth due to cell division, droplets may also
130 expand by condensation of free molecules, while cell loss due to death or migration out of the
131 imaging window is mirrored in the evaporation and shrinking of droplet sizes. Finally, by
132 analogy with the migration of cells into the field of view, new droplets may nucleate from free

133 molecules. Through this correspondence, can the statistical physics of aerosols provide insight
134 into the dynamics of cell clusters in tissues and the emergence of scaling?

135 The distribution of cluster sizes, $f(x, t)$, is the result of different sources of variability
136 including merger, fragmentation, cell division and loss. Formally, the time evolution of the
137 cluster size distribution can be cast (symbolically) as a sum of operators that describe the effect
138 of these contributions on the time evolution,

$$\partial_t f(x, t) = L_{\text{growth}}[f(x, t)] + \varphi L_{\text{fragmentation}}[f(x, t)] + \mu L_{\text{merger}}[f(x, t)] + \dots,$$

139 where the parameters, φ , μ , etc. characterize the relative strength of these processes against that
140 of growth (for details, see Supplementary Theory). To investigate the origin of scaling, we
141 questioned what determines the long-term, large-scale dependence of the cluster size
142 distribution. In statistical physics this question is typically answered by successively coarse-
143 graining the dynamics and monitoring changes in the relative contributions of different
144 processes. Under this renormalization, when a cell divides, cluster sizes are rescaled by the
145 resulting increase in tissue size, $x \rightarrow x/(1 + \delta X) \equiv \rho$. Simultaneously, time is rescaled in such
146 way that the total rate of merging and fragmentation events remains constant in this process.
147 Notably, after repeated rounds of dynamic renormalisation, the kinetic equation converges to a
148 self-similar (critical) form, where the fluctuations in cluster sizes are dominated solely by a
149 balance between merger and fragmentation events (Supplementary Theory), while the influence
150 of other processes becomes vanishingly small,

$$\partial_\tau f(\rho, \tau) \approx \varphi' L_{\text{fragmentation}}[f(\rho, \tau)] + \mu' L_{\text{merging}}[f(\rho, \tau)],$$

151 where φ' and μ' are rescaled parameters and τ is a rescaled time (Supplemental Theory).
152 Intuitively, this means that, as the organ grows, different sources of variance contribute to the
153 cluster size distribution by different degree (Fig. 2B and S1A). Crucially, in the long term,
154 contributions relating to cell fate behaviour (e.g. cell division or loss) become dominated by
155 merger and fragmentation processes, resulting in information on the former becoming erased
156 (Supplementary Theory). Therefore, while cell fate decisions affect the mean cluster size, the
157 shape of the distribution is determined entirely by merger and fragmentation events (Fig. 2C),
158 leading to the emergence of scaling behaviour observed in heart development (Fig. 1F).

159 Importantly, these results suggest not only that the cluster size distribution is entirely
160 determined by its average (scaling), but also that the shape of the distribution is independent of
161 the biological context (universality). The form of the scaling function, ϕ , relies on the
162 dependence of the merging and fragmentation rates on cluster size. In a uniformly growing
163 tissue, clone merger and fragmentation events are the result of the slow diffusive motion of
164 clusters originating from random forces exerted by the surrounding tissue (17). In this case, the
165 resulting scaling form is well-approximated by a log-normal size dependence (Fig. 2C,
166 Supplementary Theory). Indeed, such distributions are typical of merging and fragmentation
167 processes and describe the empirical distribution of droplet sizes in aerosols (18, 19). Similar
168 universal behaviour is recapitulated by a simple lattice-based Monte Carlo simulation of uniform
169 tissue growth, where the stochastic nature of cell division alone leads to merger and
170 fragmentation (Figure S1B and Supplementary Theory). Importantly, this analysis provides an
171 explanation for the observed scaling behaviour of labelled cluster sizes of mouse heart, where the
172 distribution indeed follows a strikingly log-normal size dependence (Fig. 3A,B and S2A,B). To
173 further challenge the universality of the scaling dependences, we used a similar genetic labelling

174 strategy to trace the fate of early developmental precursors in mouse liver and pancreas as well
175 as the late stage development of zebrafish heart (20). In all cases, cluster size distributions
176 showed collapse onto a log-normal size dependence (Fig. 3C-F and S2C-E), with the notable
177 exception of a subpopulation of pancreatic precursors (see below).

178 This analysis shows that, in the long term, the collective cellular dynamics leads to a
179 critical state dominated by a balance between merging and fragmentation events. The emerging
180 universal scaling distributions progressively become void of information on underlying
181 biological processes on a time scale determined by the merging and fragmentation rates. But how
182 can such information be recovered? In analogy to the turnover of adult homeostatic tissues, such
183 as interfollicular epidermis or intestine (4, 21), the behaviour of the size distribution under
184 renormalization (Fig. 2B and Supplemental Theory) shows how lineage-specific information can
185 be recovered: First, it is preserved in the non-universal cluster size dependences at short times
186 post-labelling, prior to convergence to the scaling regime. Second, convergence onto universal
187 scaling dependences is the slowest for small cluster sizes ($x \ll \langle x \rangle$). Third, if the rate of clone
188 merger is negligibly small, different cluster size distributions can emerge according to the mode
189 of cell division. The range of possible behaviours is summarised in Table 1. Finally, as merging
190 and fragmentation are emergent properties of cell fate decisions, deviations from the scaling
191 form can inform on structural properties of organ formation. As an example, in the developing
192 pancreas, acinar cells initiate from precursors localized at the tips of a complex ductal network
193 and aggregate as cohesive cell clusters thereby suppressing clonal fragmentation. This results in a
194 departure from scaling behaviour of the cluster size distribution (Figs. 3F and S2F).

195

196 In recent years, there has been a growing emphasis on genetic lineage tracing as a tool to
197 resolve the proliferative potential and fate behaviour of stem and progenitor cells in normal and
198 diseased tissues (1). Here, we have shown that the collective cellular dynamics in tissue growth
199 and turnover lead to universal clone dynamics, where cluster size distributions become
200 independent of the fate behaviour of cell populations. As well as highlighting the benefit of low-
201 density labelling and the dangers of making an unguarded assessment of clonality in lineage
202 labelled systems, these findings identify quantitative strategies to unveil cell fate-specific
203 information from short-term or small cluster size dependencies, with potential applications to
204 studies of clonal dynamics in both healthy and diseased states. At the same time, by highlighting
205 the unexpected emergence of core concepts of statistical physics in a novel context, this study
206 provides a model of how the cellular dynamics of living tissues can serve as a laboratory for
207 statistical physics.

208 **Methods**

209 **Surface area analysis of mosaically labeled hearts**

210 To generate mosaically labelled hearts at high density, *Mesp1-Cre* mice (22) were crossed with the Rosa-
211 Confetti reporter mice (23) kindly provided by Hans Clevers. Hearts collected at embryonic days E12.5
212 and P1 were fixed in 4% paraformaldehyde for 1hr at room temperature. Nuclei were counterstained with
213 Topro3 (1/500, Invitrogen). The surface images were acquired with a confocal microscope (LSM780;
214 Carl Zeiss). The surface area (SA) of each independent clusters was measured using Fiji software (24) on
215 the maximum intensity projection.

216 **Pancreas**

217 R26R-CreERT2; R26-Confetti mice were intraperitoneally injected with Tamoxifen (from Sigma) at
218 0.030mg per gram of female at E12.5 of pregnancy under Home Office guidelines, Animal Scientific
219 Procedure Act (ASPA) 1986. P14 pancreas was fixed in 4% Paraformaldehyde (PFA) overnight, and then
220 washed in PBS. Samples were sucrose-treated (30%) and mounted in OCT, and subsequently thick
221 100µm cryostat sectioned. Sections were rehydrated in PBS, blocked overnight in PBS, 2% donkey serum
222 and 0.5% Triton-100X. The samples were incubated in Dolichos biflorus agglutinin (DBA), biotinylated
223 (from Vectorlabs) for 3 days at 4°C, and AF647-Streptavidin (from Life Technologies) was applied for 2
224 days at 4°C. Next, sections were cleared with RapiClear 1.52 (from SunJin Lab). Images were acquired
225 with Leica TCS SP5 confocal microscope, using the tiling mode. The images were analyzed with
226 Volocity and volumes and coordinates of centers of clonal clusters quantified. To obtain 3D
227 reconstructions from Z stacks obtained with Leica SP5 microscope, Imaris (v8, Bitplane) was used.

228 **Liver**

229 R26R-CreERT2⁺;Rainbow⁺ mice were a kind gift from Magdalena Zernicka-Goetz (University of
230 Cambridge, UK). R26R-CreERT2⁺;Rainbow⁺ male mice were crossed with wild-type MF1 females and
231 labelling induced by intraperitoneal injection of pregnant dams with Tamoxifen (Sigma). Tamoxifen was
232 prepared at 10 mg/mL in sunflower oil and induction performed using 0.025 mg Tamoxifen per gram of
233 pregnant dam. Pregnant dams were induced at E9.5 and the resulting pups had livers collected at postnatal
234 day P30 – P45. Livers were divided into pieces of thickness ~10mm, washed at least 3 times in PBS to
235 remove blood and fixed in 4% Paraformaldehyde overnight before being washed twice in PBS. Liver
236 pieces were mounted in 4% Low Melt Agarose (Bio-Rad) and 100µm thick sections cut using a
237 vibratome (Leica VT1000 S). Thick sections were stored in PBS at 4 °C before immunostaining. Briefly,
238 sections were blocked in PBS + 5% DMSO (Sigma) + 2% donkey serum (Sigma) + 1% Triton-X100
239 (Sigma) overnight before incubation in PBS + 1% DMSO + 2% donkey serum + 0.5% Triton-X100 +
240 1:40 goat anti-Osteopontin (R&D Systems, AF808) for 3 days at 4 °C. Following several washes in PBS
241 + 1% DMSO + 0.5% Triton-X100 at 4 °C for 24 h, sections were incubated in PBS + 1% DMSO + 2%

242 donkey serum + 0.5% Triton-X100 + 1:250 donkey anti-goat antibody conjugated to AF647 (Life
243 Technologies) for 2 days at 4 °C. Following the staining, sections were cleared by increasing glycerol
244 gradient before incubation with PBS + 1:1000 Hoechst 33342 (Sigma) for 1h at 4 °C to counterstain
245 nuclei and mounted with Vectashield (Vector Laboratories). Images of liver sections were acquired using
246 a Leica TCS SP5 confocal microscope and processed using LAS AF Lite software (Leica). Cell numbers
247 for each labelled cluster were counted manually from acquired images.

248 **Code availability**

249 Custom code used to in this study is available from the corresponding authors upon reasonable
250 request.

251 **Data availability**

252 The data that support the plots within this paper and other finding of this study are available from
253 the corresponding author upon request.

254

255

256 **References and Notes:**

- 257 1. K. Kretzschmar, F. M. Watt, Lineage tracing. *Cell*. **148**, 33–45 (2012).
- 258 2. C. Blanpain, B. D. Simons, Unravelling stem cell dynamics by lineage tracing. *Nat. Rev. Mol. Cell*
259 *Biol.* **14**, 489–502 (2013).
- 260 3. S. J. Morrison, A. C. Spradling, Stem Cells and Niches: Mechanisms That Promote Stem Cell
261 Maintenance throughout Life. *Cell*. **132**, 598–611 (2008).
- 262 4. A. M. Klein, B. D. Simons, Universal patterns of stem cell fate in cycling adult tissues.
263 *Development*. **138**, 3103–11 (2011).
- 264 5. S. Rulands, B. D. Simons, Tracing cellular dynamics in tissue development, maintenance and
265 disease. *Curr. Opin. Cell Biol.* **43**, 38–45 (2016).
- 266 6. A. M. Klein, D. P. Doupé, P. H. Jones, B. D. Simons, Mechanism of murine epidermal
267 maintenance: Cell division and the voter model. *Phys. Rev. E*. **77**, 31907 (2008).
- 268 7. A. Bondue, C. Blanpain, Mesp1: A Key Regulator of Cardiovascular Lineage Commitment. *Circ.*
269 *Res.* **107**, 1414–1427 (2010).
- 270 8. F. Lescroart *et al.*, Early lineage restriction in temporally distinct populations of Mesp1
271 progenitors during mammalian heart development. *Nat. Cell Biol.* **16**, 829–840 (2014).
- 272 9. S. Chabab *et al.*, Uncovering the Number and Clonal Dynamics of Mesp1 Progenitors during
273 Heart Morphogenesis. *Cell Rep.* **14**, 1–10 (2016).
- 274 10. A. Wuidart *et al.*, Quantitative lineage tracing strategies to resolve multipotency in tissue-specific
275 stem cells. *Genes Dev.* **30**, 1261–1277 (2016).
- 276 11. S. M. Meilhac *et al.*, A retrospective clonal analysis of the myocardium reveals two phases of
277 clonal growth in the developing mouse heart. *Development*. **130**, 3877–89 (2003).
- 278 12. D. Sedmera, R. P. Thompson, Myocyte proliferation in the developing heart. *Dev. Dyn.* **240**,
279 1322–34 (2011).
- 280 13. L. Foret *et al.*, A General Theoretical Framework to Infer Endosomal Network Dynamics from
281 Quantitative Image Analysis. *Curr. Biol.* **22**, 1381–1390 (2012).

- 282 14. P. L. Krapisky, S. Redner, E. Ben-Naim, *A Kinetic View of Statistical Physics* (Cambridge
283 University Press, Cambridge, 2010).
- 284 15. S. K. Friedlander, *Smoke, Dust, and Haze* (Oxford University Press, Oxford, 2000).
- 285 16. E. M. Hendriks, M. H. Ernst, R. M. Ziff, Coagulation equations with gelation. *J. Stat. Phys.* **31**,
286 519–563 (1983).
- 287 17. J. Ranft *et al.*, Fluidization of tissues by cell division and apoptosis. *Proc. Natl. Acad. Sci. U. S. A.*
288 **107**, 20863–8 (2010).
- 289 18. S. Redner, in *Disorder and Fracture*, J. C. Charmet, S. Roux, E. Guyon, Eds. (Springer US,
290 Boston, MA, 1990), vol. 204 of *NATO ASI Series*.
- 291 19. S. K. Friedlander, C. S. Wang, The self-preserving particle size distribution for coagulation by
292 brownian motion. *J. Colloid Interface Sci.* **22**, 126–132 (1966).
- 293 20. V. Gupta, K. D. Poss, Clonally dominant cardiomyocytes direct heart morphogenesis. *Nature.* **484**,
294 479–84 (2012).
- 295 21. E. Clayton *et al.*, A single type of progenitor cell maintains normal epidermis. *Nature.* **446**, 185–9
296 (2007).
- 297 22. Y. Saga *et al.*, MesP1 is expressed in the heart precursor cells and required for the formation of a
298 single heart tube. *Development.* **126**, 3437–47 (1999).
- 299 23. H. J. Snippert *et al.*, Intestinal crypt homeostasis results from neutral competition between
300 symmetrically dividing Lgr5 stem cells. *Cell.* **143**, 134–44 (2010).
- 301 24. J. Schindelin *et al.*, Fiji: an open-source platform for biological-image analysis. *Nat. Methods.* **9**,
302 676–682 (2012).
- 303 24. P. Olesen *et al.*, Diffusion, fragmentation, and coagulation processes: Analytical and numerical
304 results. *Phys. Rev. E* **72**, 031103 (2006)
- 305

306 **Acknowledgements:**

307 B.D.S. acknowledges the support of the Wellcome Trust (grant number 098357/Z/12/Z). F.L. is supported
308 by a long-term EMBO fellowship and the postdoctoral fellowship of the FNRS. S.C. is supported by a
309 FRIA/FNRS fellowship. C.B. is supported by the ULB, a research grant of the FNRS, the foundation
310 Bettencourt Schueller, the Foundation ULB and the Foundation Baillet Latour. M.S. is supported by an
311 MRC doctoral training award and A.P. is supported by MRC Research grant MR/K018329/1. M.H. is a
312 Wellcome Trust Sir Henry Dale Fellow and is jointly funded by the Wellcome Trust and the Royal
313 Society (104151/Z/14/Z); M.H. and N.P. are funded by a Horizon 2020 grant (LSFM4LIFE). C.H. was
314 funded by a Cambridge Stem Cell Institute Seed funding award for interdisciplinary research awarded to
315 M.H. and B.D.S.. We are grateful to Kenneth D. Poss and Vikas Gupta for making a digital version of
316 their data available to us.

317

318 **Author contributions:**

319 S.R. and B.D.S. conceived the project. S.C., F.L., C.J.H., N.P., and M.S. performed the experiments and
320 collected the raw data. M.H. supervised the liver experiments. S.R. developed the theory, performed the
321 modelling and statistical analysis. S.R. and B.D.S. drafted the manuscript. All authors edited and approved
322 the final manuscript.

323 **Competing financial interests:** The authors declare no competing financial interests.

324 **Data availability statement:** The data that support the findings of this study are available from the
325 corresponding author upon reasonable request.

326

327 **Ethical statement:** We have complied with all relevant ethical regulations. Mesp1-Cre mice colonies
328 were maintained in a certified animal facility in accordance with European
329 guidelines. These experiments were approved by the local ethical committee
330 under the reference #LA1230332(CEBEA). Research using mice for pancreas and liver samples has been
331 regulated under the Animal (Scientific Procedures) Act 1986 Amendment Regulations 2012 following
332 ethical review by the University of Cambridge Animal Welfare and Ethical Review Body (AWERB).
333 These experimental data sets were obtained as by-products from other research projects undertaken by the
334 respective laboratories.

335

337 **Fig. 1. Clonal dynamics during tissue development.** (A) Lineage tracing allows resolving clonal
338 dynamics using a “two-time” measurement in living organisms. (B) Merger and fragmentation of labelled
339 cell clusters occur naturally because of large-scale tissue rearrangements during the growth and
340 development of tissues. (C,D) Illustration of clone fragmentation in mouse during the development of (C)
341 liver and (D) pancreas (collection at post-natal day (P)45 and P14, respectively) following pulse-labelling
342 using, respectively, R26R-CreERT2;Rainbow and R26R-CreERT2; R26-Confetti at E9.5 and E12.5,
343 respectively. Portal tracts (PT) and central veins (CV) are highlighted in white, osteopontin (a ductal
344 marker) is shown in purple and nuclei are marked in blue. Pancreatic ducts are shown in grey. (E) High
345 density (mosaic) labelling of mouse heart using the Mesp1-Confetti system showing the left/right atrium
346 (L/RA), left/right ventricle (L/RV) and the in/out-flow tracts (I/OFT). (F) Distributions of cell cluster
347 sizes on the surface of the developing mouse heart at E12.5 (680 clusters from 4 mice) and P1 (373
348 clusters from 3 mice). (G) Average cluster sizes in different heart compartments and time points during
349 development. Error bars denote 95% confidence intervals. (H) Rescaled cluster size distributions showing
350 scaling behaviour.

351

352 **Fig. 2. Origin of scaling and universality in clonal dynamics during development.** (A) Sizes of
353 labelled cell clusters in developing tissues are determined by processes analogous to the kinetics of
354 droplets in aerosols, as depicted. (B) Sketch of the renormalisation flow diagram showing how the
355 relative contributions of different processes to the cluster size distribution evolve during development. At
356 long times and/or larger cluster sizes, the time evolution of the cluster size distribution becomes
357 controlled by three fixed points (dependent on the details of the merging and fragmentation processes),
358 where it acquires a universal scaling dependence (Supplementary Information). The inset shows a
359 schematic of the renormalization process, with the largest cluster sizes (grey) converging more rapidly
360 onto the universal distribution than the smallest cluster sizes (red). (C) Rescaled cluster size distributions
361 for different division modes obtained by numerical simulations (Supplemental Theory) collapse onto a
362 universal log-normal form (grey line).
363

364 **Fig. 3. Universality of cluster sizes in different tissue types and organisms.** (A-B) Cumulative cluster
365 size distributions obtained from lineage tracing studies of the mouse heart. (C-E) Experimental
366 cumulative cluster size distributions for (C) mouse liver (892 clusters from 4 mice), (D) mouse pancreas
367 (988 clusters from 3 mice), and (E) zebrafish heart (from (20)) collapse onto the predicted universal log-
368 normal dependence fitted by maximum likelihood estimation (grey). Data shown in colour and shading
369 shows 95% Kolmogorov confidence intervals. (F) Experimental cumulative cluster size distributions
370 (solid lines) separated by time, region, cell type labelling strategy collapse onto a universal shape (dashed
371 line) with the exception of a subset of pancreatic acinar cells (inlay).
372

373 **Table 1. Non-universal dependencies of the cluster size distribution.** Analytical expressions for the
374 cluster size distribution (top row in each cell) and average cluster size (bottom row). Shown are
375 expressions in situations, where labelling density is clonal, labelling density is almost clonal but clones
376 are subject to fragmentation, and where both merging and fragmentation of clones occur (left to right). As
377 merging and fragmentation both result from tissue rearrangements merging should always imply
378 fragmentation. Time is measured in units of the cell cycle time. Expressions are valid after convergence to
379 the scaling regime, when the typical cluster size is much larger than the size of single cells, and in the
380 mean-field limit, which is a good approximation for two and three dimensional tissues. In addition, it is
381 assumed that the full spectrum of cluster sizes can be experimentally resolved. If clones fragment but not
382 merge fragmentation and growth ultimately compensate to lead to a stationary distribution. In case of
383 clonal merging and fragmentation expressions give empirical approximations, where α depends on the
384 details of the merging and fragmentation processes (see Supplemental Theory).

385

386

387

388

Fig. 1

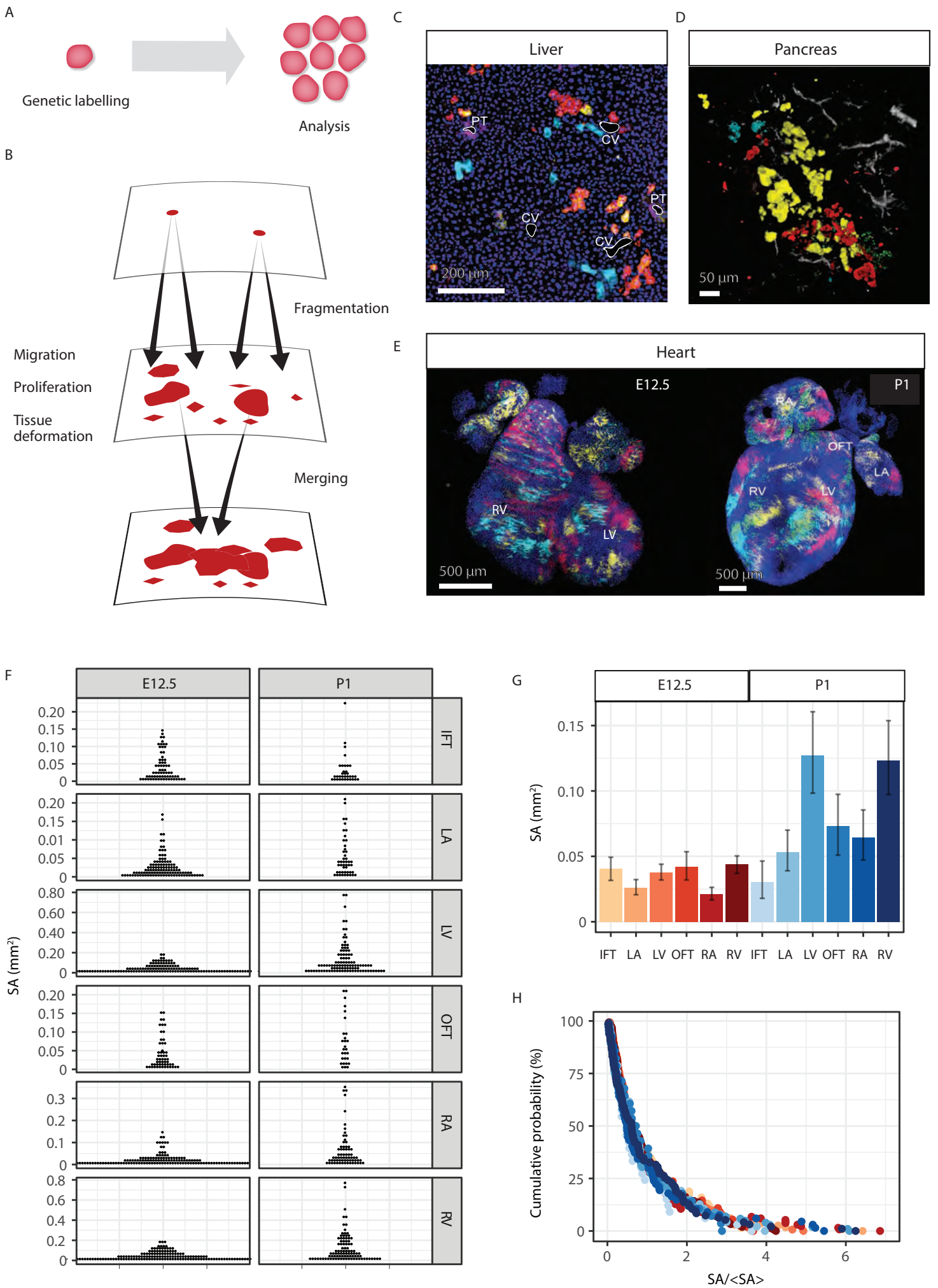


Fig. 2

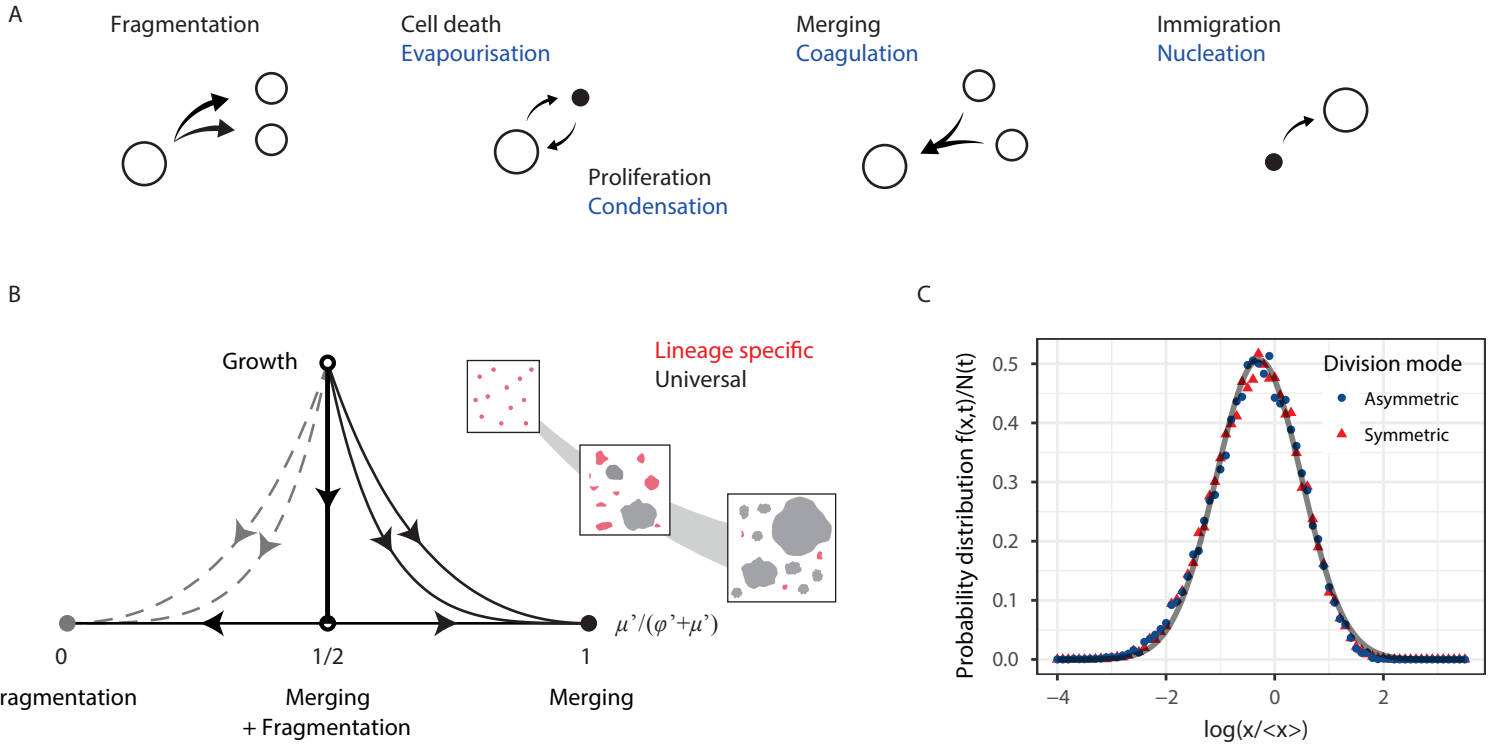


Fig. 3

